ANL/EVS-21/8

Coupled Ocean Wave-Atmosphere Models

For Offshore Wind Energy Applications

Environmental Science Division

Offshore Wind Resource Sciences FY2021 Q1 Report

This report is prepared for the Offshore Wind Resources Sciences AOP Project (Direct-Funded Lab Project).
Current Year CPS Agreement Number: 34145

ANL/EVS-21/8

Coupled Ocean Wave-Atmosphere Models

For Offshore Wind Energy Applications

prepared by
William J. Pringle
Veerabhadra R. Kotamarthi

Environmental Science Division, Argonne National Laboratory

prepared for:
Offshore Wind Resource Sciences AOP Project,
Wind Energy Technologies Office, Department of Energy

May 28, 2021

1 Abstract

Coupling ocean wave models to mesoscale atmospheric models is necessary to represent the effect of waves on wind turbine hub-height winds. In this report we provide a review of the most widely used ocean waves models and the phased-averaged spectral wave modeling paradigm that they are based on. Methodologies used to couple these wave models to mesoscale atmospheric models are described along with details of existing coupled modeling systems. We summarize impacts on offshore wind resource assessments that have been investigated with such coupled modeling systems to-date. Specifically, coupling in the North and Baltic Seas was shown to have a small negative effect on the offshore wind energy resource at weak-to-moderate wind speeds, with little impact at higher wind speeds. Finally, limitations of these existing coupled modeling systems and impact assessments are discussed, including examples of and the potential for improved parameterizations of the air-sea fluxes, and the use of fine-scaled simulations using phased-resolved wave models.

2 Introduction

The marine atmospheric boundary layer (MABL) is characterized by a high Reynolds number stratified flow, and a dynamic bottom boundary at the air-sea interface shaped by surface ocean gravity waves (Sullivan & McWilliams, 2010). For offshore wind energy applications it is important to be able to accurately model the MABL, especially at the wind turbine hub height, under a wide variety of metocean conditions. The result of this modeling is used for offshore wind resource assessment, site selection, wind turbine and farm design, and installation, maintenance and decommission planning (Kalvig, Gudmestad, & Winther, 2014; Veers et al., 2019). However, the marine environment brings a number of particular modeling challenges compared to the terrestrial environment. For instance, typically the MABL exhibits much shallower depths than those occurring over land, hence the effect of the surface is felt though a higher percentage of the MABL (Patton et al., 2019).

Observations and turbulence simulations indicate that ocean waves impact boundary layer winds by imparting an upward flux of momentum from the ocean to the atmosphere (Patton et al., 2019). Therefore, a model should intuitively account for the two-way air-sea interaction to properly describe the surface layer, especially for forecast lead times greater than a couple of days (Deskos, Lee, Draxl, & Sprague, 2021). Various two-way coupled mesoscale models have been developed over the years, as we describe in this report, although so far with limited application to offshore wind energy. But even with such capabilities, significant modeling uncertainty of the coupled metocean environment remains, such as with regards to swell waves, breaking and irregular waves, atmospheric stability and tropical storms (Patton et al., 2019; Veers et al., 2019). Reasons for modeling uncertainty includes theoretical deficiencies, such as description of the surface layer based on Monin-Obukhov similarity theory (Monin & Obukhov, 1954; Sullivan & McWilliams, 2010), the related wind-wave equilibrium assumption that is generally not achieved in coastal zones where offshore turbines are likely to be located (Patton et al., 2019), and spectral-based descriptions of

surface gravity wave generation, breaking, and nonlinear interactions (Cavaleri, Barbariol, Benetazzo, & Waseda, 2019). In addition, there are significant technical challenges as related to model coupling between different physics (atmosphere circulation, ocean circulation, and surface ocean gravity waves), and across multiple scales (mesoscale-to-microscale; Haupt et al., 2019; Veers et al., 2019).

In this report, we start by describing phase-averaged spectral wave modeling and the two most widely used models (Sect. 3). In Sect. 4 we describe mesoscale coupled atmosphere-wave-ocean models and the methods used to account for the effect of waves and ocean circulation on the air-side interfacial stress, and the impacts of coupling of the limited applications to offshore resource assessment. Lastly, we discuss the coupled model assessments and their limitations and make suggestions for future research directions on this topic (Sect. 5).

3 Phase-Averaged Spectral Wave Modeling

3.1 Introduction

According to linear wave theory the sea surface elevation of waves (ζ) at one point as a function of time (t) is equal to the summation of all individual waves of a certain amplitude (a), ocean current-relative angular frequency (σ), and random phase (α),

$$\zeta = \sum_i a_i \cos\left(\sigma_i t + \alpha_i\right) \tag{1}$$

And under the linear wave theory approximation of slowly varying current and depth, the following dispersion relation and Doppler-type equation to interrelate the phase parameters can be applied,

$$\sigma^2 = gk \tanh(kd) \tag{2}$$

$$\omega = \sigma + \mathbf{k} \cdot \mathbf{U} \tag{3}$$

where d is the mean depth, $\mathbf{U}$ is the depth-averaged current vector, g is the acceleration of gravity, and $\mathbf{k}$ is the wavenumber vector with magnitude k and direction θ.

However, wind waves in the ocean have periods of order seconds and wavelengths of order meters. Thus, resolving each individual wave in the ocean over wide spatial scales, such as those of mesoscale weather systems, would be inordinately expensive to simulate. To remove this obstacle to computation, spectral wave models have been developed that simulate the integrated wave energy spectrum, E, instead of the time-space evolution of the sea surface elevation. This also has the advantage that many properties are the sea state are better understood from this spectral perspective. In the presence of ocean currents, it is the wave action density $N \equiv E/\sigma$ that is conserved, rather than E. The corresponding governing equation of conservation of N is known as the spectral action density balance equation (or just action balance equation),

$$\frac{DN}{Dt} = \frac{S}{\sigma} \tag{4}$$

where $\frac{D}{Dt}$ represents the total derivative (moving with a wave component), and S represents the net effect of sources and sinks for the wave spectrum. Source terms include parameterizations for such physical processes as wave growth due to the actions of wind, nonlinear resonant wave-wave interactions, scattering due to wave-bottom interactions, triad interactions, and dissipation due to whitecapping, bottom friction, surf-breaking, and interactions with vegetation, mud and ice (WW3DG, 2019).

The implicit assumption of equation (4) is that properties of the medium (water depth and current), as well as the wave field itself, vary on time and space scales that are much larger than the variation scales of a single wave (WW3DG, 2019). Another practical reason for using spectral wave models is that mesoscale atmospheric models operate at far greater spatial scales [O(100-m) to O(10-km)] than individual wind waves. Therefore, there is practically little to be gained from resolving the individual waves at sub-grid scales of the weather model since the surface stresses do not vary within the computational cell.

Finally, while the wave spectra N is the quantity that is simulated, it is converted to more practically useful quantities on model output. The most important of those is known as the significant wave height, H_s, defined traditionally as the wave heights of the highest 1/3rd waves in the spectrum, or in more modern terms as four times the standard deviation of the sea surface elevation. Other commonly output quantities are the mean wave period (various definitions; T_{m02}, $T_{m0,-1}$, or $T_{m0,1}$), mean wavelength (L_m), mean wave direction (θ_m), peak frequency and direction, and the phase speed, wave length, and period at the peak frequency (WW3DG, 2019).

3.2 WAVEWATCH III

WAVEWATCH III (WW3) solves the random phase spectral action density balance equation (4) for wavenumber-direction spectra, $N_k \equiv N(k, \theta; \mathbf{x}, t)$, which is a key unique feature of WW3. This is because the wavenumber-direction spectrum is invariant with respect to physics of wave growth and decay for variable water depths (WW3DG, 2019). The resulting Eulerian form of (4) that WW3 solves is given as,

$$\frac{\partial N_k}{\partial t} + \nabla_x \cdot (\dot{\mathbf{x}} N_k) + \frac{\partial}{\partial k}(\dot{k} N_k) + \frac{\partial}{\partial \theta}(\dot{\theta} N_k) = \frac{S}{\sigma}, \tag{5}$$

$$\dot{\mathbf{x}} = \mathbf{c}_g + \mathbf{U}, \tag{6}$$

$$\dot{k} = -\frac{\partial \sigma}{\partial d}\frac{\partial d}{\partial s} - \mathbf{k} \cdot \frac{\partial \mathbf{U}}{\partial s}, \tag{7}$$

$$\dot{\theta} = -\frac{1}{k}\left[\frac{\partial \sigma}{\partial d}\frac{\partial d}{\partial m} + \mathbf{k} \cdot \frac{\partial \mathbf{U}}{\partial m}\right], \tag{8}$$

where ∇_x represents the two-dimensional spatial differential operator, $\mathbf{c}_g = (c_g \sin\theta, c_g \cos\theta)$, s is a coordinate in the direction θ, m is a coordinate perpendicular to s, and c_g is the group velocity,

$$c_g = \frac{\partial \sigma}{\partial k} = \left[\frac{1}{2} + \frac{kd}{\sinh(2kd)}\right]\frac{\sigma}{k} \tag{9}$$

The governing equations (5)-(8) can be solved in either Cartesian coordinates or spherical coordinates, the latter for large-scale problems. First-, second- and third-order accurate numerical schemes are available, on either regular (rectilinear or curvilinear) or unstructured (triangular) grids, individually or combined into multi-grid mosaics (WW3DG, 2019). Regular grids are mostly used, but recent improvements to the computational performance and scalability of WW3 on unstructured triangular grids have been made by using parallel domain decomposition (Abdolali et al., 2020). This is especially useful for modeling the cross-scale wave dynamics from the nearshore to offshore, and for coupling to unstructured grid hydrodynamic coastal ocean models to simulate extreme storm events (e.g., hurricanes) where coastal waves and surge are of primary concern.

Traditionally, WW3 is solved using an explicit fractional step method, where the equations are split into different components each with their own time step. The different components are the intra-spectral propagation, spatial propagation, and source term integration. Intra-spectral propagation is required due to the way the wavenumber grid is discretized in WW3, which is variable according the water depth to account for the change in wavenumber due to shoaling in shallow water. This explicit scheme is limited by the Courant-Friedrichs-Lewy (CFL) condition which can lead to inefficiency when concurrently modeling the nearshore and offshore wave physics. To alleviate this potential inefficiency, an implicit time-integration scheme, which only requires a single global time step and no equation splitting, was recently implemented in WW3 (Abdolali et al., 2020).

3.3 SWAN

The Simulating Waves Nearshore (SWAN) solves the random phase spectral action density balance equation (4) for frequency-direction spectra, $N_\sigma \equiv N(\sigma, \theta; \mathbf{x}, t)$, in contrast to the wavenumber-direction spectra used in WW3. The resulting Eulerian form of (4) that SWAN solves is given as (The SWAN team, 2020),

$$\frac{\partial N_\sigma}{\partial t} + \nabla_x \cdot (\dot{\mathbf{x}} N_\sigma) + \frac{\partial}{\partial \sigma}(\dot{\sigma} N_\sigma) + \frac{\partial}{\partial \theta}(\dot{\theta} N_\sigma) = \frac{S}{\sigma}, \tag{10}$$

$$\dot{\mathbf{x}} = \mathbf{c}_g + \mathbf{U}, \tag{11}$$

$$\dot{\sigma} = \frac{\partial \sigma}{\partial d}\left[\frac{\partial d}{\partial t} + \mathbf{U} \cdot \nabla_x d\right] - c_g \mathbf{k} \cdot \frac{\partial \mathbf{U}}{\partial s}, \tag{12}$$

$$\dot{\theta} = -\frac{1}{k}\left[\frac{\partial \sigma}{\partial d}\frac{\partial d}{\partial m} + \mathbf{k} \cdot \frac{\partial \mathbf{U}}{\partial m}\right], \tag{13}$$

with the same variable definitions as for WW3 in Sect. 3.2. The governing equations (10)-(13) can be solved in either Cartesian coordinates or spherical coordinates, the latter for large-scale problems. The equations can be solved on either regular or unstructured triangular grids. The finite-difference numerical method is used with a first-order upwind, backward space, backward time scheme, or a second-order BDF or cyclic scheme. These implicit numerical schemes in SWAN are unconditionally stable and high Courant numbers can be adopted. Among other reasons, this is a key advantage of SWAN as it can

efficiently simulate waves nearshore and offshore simultaneously. However, since energy propagates along a wave ray and these wave rays can become curved in coastal waters from depth changes and ambient currents, an iterative process is required to solve the system of equations for a single time step (The SWAN team, 2020).

4 Coupling Waves to Mesoscale Atmospheric Models

Spectral wave models, like those described in Sect. 3, are often coupled to mesoscale atmospheric models. In fact, a number of coupled atmosphere-wave-ocean modeling systems have been developed that can provide background level quantities of low-level winds, wind-waves, and ocean surface currents that characterize the offshore wind energy environment (e.g., Chen, Price, Zhao, Donelan, & Walsh, 2007; Li, Curcic, Iskandarani, Chen, & Knio, 2019; Liu, Liu, Xie, Guan, & Zhao, 2011; Warner, Armstrong, He, & Zambon, 2010; L. Wu, Breivik, & Rutgersson, 2019; J. Zhang, Huang, Wen, & Deng, 2009). Within these coupled modeling systems, the determination of the air-side interfacial stress between the atmosphere and the ocean, τ, is one of the most important components. Although it is likely valid only in pure wind-driven seas (Drennan, Graber, Hauser, & Quentin, 2003), we typically invoke Monin-Obukhov similarity theory (MOST; Monin & Obukhov, 1954) to approximate the surface layer. Under neutral stability conditions, MOST implies that the horizontal surface velocity of the atmosphere, u, follows a logarithmic profile with vertical height above the surface, z,

$$u = \frac{u_*}{\kappa} \ln \frac{z}{z_0} \tag{14}$$

where, $\kappa = 0.4$ is the von Karman constant, z_0 is the surface roughness height, or more specifically, the height at which the velocity is artificially zero, and u_* is the friction velocity such that $\tau \equiv \rho_a u_*^2$, in which ρ_a is the air density. Usually, the neutral 10-m wind speed, U_{10}, is used with (14) leading to the bulk aerodynamic drag equation that is often used to approximate surface fluxes (Deskos et al., 2021),

$$\tau = \rho_a C_d U_{10}^2 \tag{15}$$

$$C_d = \left[\frac{\kappa}{\ln(\frac{10}{z_0})} \right]^2 \tag{16}$$

where C_d is known as the drag coefficient. In the case that the atmospheric model is being used stand-alone without coupling to ocean waves, z_0 is often approximated by the standard Charnock equation (Charnock, 1955),

$$z_0 = z_{ch} \frac{u_*^2}{g} + \frac{\nu}{u_*} \tag{17}$$

where ν is the kinematic viscosity of air, z_{ch} is the dimensionless Charnock parameter, which is suggested to set to 0.011 in the open ocean and 0.034 for near coastal waters

(Kalvig et al., 2014), 0.016 for rapidly rising seas (Warner et al., 2010), or computed as $z_{ch} = 0.011 + 0.007 \min[\max[(U_{10} - 10)/8, 0)], 1.0]$ (L. Wu et al., 2019).

Many formulations have been proposed that build on the above concepts to incorporate the effects of waves on z_0. These can be based on wave-age (e.g., Drennan et al., 2003; Oost, Komen, Jacobs, & Van Oort, 2002), sea-spray (e.g., Makin, 2005), significant wave height and length (e.g., Taylor & Yelland, 2001), or directional wave spectra (e.g., Janssen, 1991). Additional considerations based on the relative direction of wind and swell have also been explored (Patton et al., 2019), which in a simplistic sense can decrease (wind following swell) or increase (wind opposing swell) the effective sea surface drag (Kalvig et al., 2014). The following sections provide an overview of some implemented coupled atmosphere-ocean-wave modeling systems, and their proposed methods for computing z_0. A generalized overview of these coupling modeling systems is illustrated in Fig. 1.

4.1 COAWST

The Coupled Ocean–Atmosphere–Wave–Sediment Transport (COAWST) Modeling System (Warner et al., 2010) is one of the most mature modeling systems coupling mesoscale atmospheric models with spectral wave models. It also couples these two modules with ocean circulation, sediment transport, and sea-ice models as required. COAWST has been often used for tropical cyclone research (e.g., Olabarrieta, Warner, Armstrong, Zambon, & He, 2012; Warner et al., 2010; R. Wu, Zhang, Chen, Li, & Lin, 2018; Zambon, He, & Warner, 2014).

COAWST is comprised of the Regional Ocean Modeling system (ROMS) (Shchepetkin & McWilliams, 2005) for ocean circulation, Weather Research and Forecasting (WRF) model (Powers et al., 2017) for the atmosphere, and either SWAN (Sect. 3.3) or WW3 (Sect. 3.2) for waves; in addition to sediment transport and sea-ice models which we will not discuss here (Sutil & Pezzi, 2020). SWAN is the original wave model component of COAWST (Warner et al., 2010), while WW3 has been more recently added, likely due its advanced wave-ice interaction features. These modules are linked through the Modeling Coupling Toolkit (MCT) (Jacob, Larson, & Ong, 2005; Larson, Jacob, & Ong, 2005) which interpolates and exchanges the following interfacial quantities (Warner et al., 2010):

- WRF → ROMS: 10-m wind velocities, shortwave and longwave net heat fluxes, atmospheric pressure, relative humidity, air temperature, cloud fraction, precipitation;
- ROMS → WRF: sea surface temperature;
- SWAN/WW3 → ROMS: wave direction, surface and bottom wave periods, percent wave breaking, wave energy dissipation, bottom orbital velocity;
- ROMS → SWAN/WW3: sea surface elevation, surface currents;
- SWAN/WW3 → WRF: significant wave heights and length;
- WRF → SWAN/WW3: 10-m wind velocities.

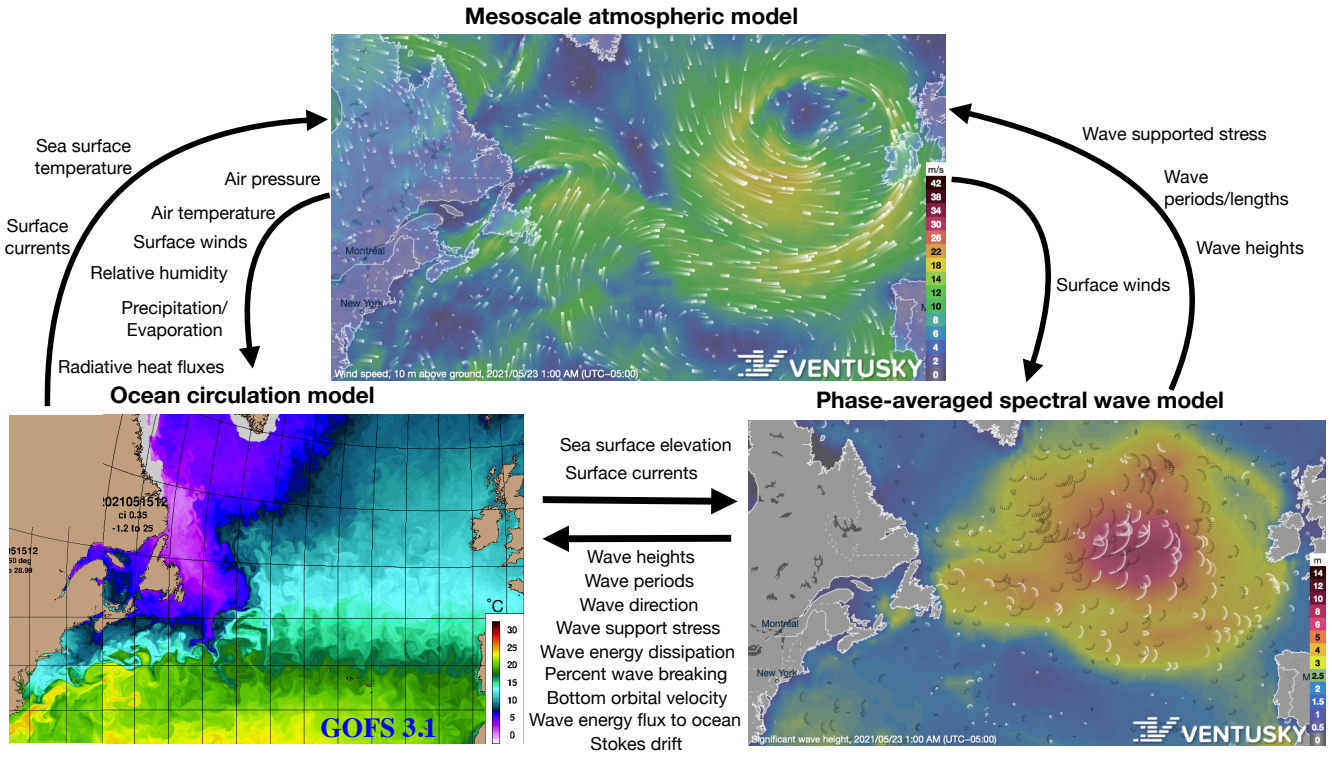

Figure 1: Illustration of outputs and interactions between components of a coupled mesoscale atmosphere-ocean-wave modeling system; panels show model outputs over the North Atlantic for May 23, 2021. A range of variables that are typically exchanged between the models are shown, some of which may or may not be used depending on the specifics of the models and parameterizations. Sources: Ventuksy (`https://www.ventusky.com/`) for the top panel showing wind speeds and the bottom right panel showing wave heights; Global HYCOM+CICE system (GOFS 3.1) (`https://www7320.nrlssc.navy.mil/GLBhycomcice1-12/skill.html`) for the bottom left panel showing sea surface temperature.

Focusing on the SWAN/WW3 → WRF exchange, the computed wave properties are being used to provide an estimate of ocean surface roughness, and hence the air-side interfacial stress, in lieu of the Charnock approximation, Eq. (17). COAWST has used a few formulations to estimate z_0 for use in Eq. (14). The first (Warner et al., 2010) uses Taylor and Yelland (2001)'s formulation,

$$z_0 = 1200 H_s \left(\frac{H_s}{L_m} \right)^{4.5} + 0.11 \frac{\nu}{u_*} \tag{18}$$

where H_s is the significant wave height and L_m is the mean wavelength (see Sect. 3.1). The above formulation was compared with wave-age based formulations in Olabarrieta et al.

(2012),

$$z_0 = 3.35 H_s \left(\frac{u_*}{C_p}\right)^{3.4} \text{(Drennan et al., 2003), and;} \tag{19}$$

$$z_0 = \frac{25}{\pi} L_p \left(\frac{u_*}{C_p}\right)^{4.5} \text{(Oost et al., 2002)} \tag{20}$$

where C_p and L_p are the phase speed and wave length at the peak frequency, respectively (see Sect. 3.1). Note also that Olabarrieta et al. (2012) replaced L_m with L_p in (18).

4.2 UU-CM

The Uppsala University Coupled model (UU-CM) is a coupled ocean-wave-atmosphere model designed for the Baltic Sea and the North Sea (L. Wu et al., 2019; L. Wu, Shao, & Sahlée, 2020). UU-CM is comprised of the Nucleus of European Modelling of the Ocean (NEMO) for the ocean (Bourdallé-Badie et al., 2019), WRF for the atmosphere, and WW3 (Sect. 3.2) for waves. These modules are coupled together using the OASIS-MCT coupling toolkit (Craig, Valcke, & Coquart, 2017), with the following variables exchanged (L. Wu et al., 2019):

- WRF → NEMO: atmospheric wind stress, shortwave and longwave radiation, net water flux (precipitation minus evaporation);
- NEMO → WRF: sea surface temperature, ocean surface currents;
- WW3 → NEMO: significant wave height, mean wave period, wave supported stress, momentum flux from waves to currents, Stokes drift;
- NEMO → WW3: sea surface elevation, ocean surface currents;
- WW3 → WRF: wave supported stress;
- WRF → WW3: 10-m wind velocities.

Similar to COAWST, the computed wave properties are used to provide an estimate of z_0 and hence the air-side interfacial stress. UU-CM uses the Charnock equation (17) to compute z_0 but incorporates the effects of waves in the computation of z_{ch} (Janssen, 1991),

$$z_{ch} = \frac{\alpha}{\sqrt{1 - \tau_w/\tau}} \tag{21}$$

where $\alpha = 0.0095$, and τ_w is the wave supported stress from the directional wave spectra,

$$\tau_w = \rho_w g \int_0^{2\pi} \int_0^{\infty} \frac{\mathbf{k}}{\omega} S_{in} d\omega d\theta \tag{22}$$

where ρ_w is the density of water, and S_{in} is the wind input source term, which is a component of S in Eq. (4). We note that another two-way coupled atmosphere-ocean wave system

called CHAOS (Chemical Hydrological Atmospheric Ocean wave System), developed for the Mediterranean and Black Seas uses the same formulation as above to estimate z_0 (Varlas, Katsafados, Papadopoulos, & Korres, 2018; Varlas, Spyrou, Papadopoulos, Korres, & Katsafados, 2020).

An additional effect on the computation of the air-side stress in UU-CM is that the wind speed in (15) is based on the vector difference between the 10-m wind velocity and ocean surface currents, therefore both the ocean model and the wave model can directly affect the computation of τ.

4.3 Coupling Impacts on Offshore Wind Resource Assessments

Using UU-CM in the North and Baltic Seas it was found that coupling processes affected the offshore wind power density by less than ∼6% (L. Wu et al., 2020). Interestingly, atmosphere-ocean coupling had a larger effect than atmosphere-wave coupling on the wind power density. In fact, difference in wind power density to a stand-alone atmospheric model was greater for the coupled atmosphere-ocean setup than the fully coupled atmosphere-wave-ocean simulation. This is because the mean 10-m wind speed tends to be reduced with atmosphere-wave coupling due to a slightly higher drag coefficient under moderate wind conditions (L. Wu et al., 2019). Similarly, Varlas et al. (2018) also found an estimated 12% reduction to wind speeds when coupling. Overall, it was found that the fully coupled simulation estimated wind power densities to within ±2% to the stand-alone atmospheric model during January 2015, but percent greater differences in July 2015 (±6%). However, the magnitude of the wind power density was far greater during January. It is noted that the effect of coupling on the wave potential energy was much larger (up to 25%) than the effect on the wind power density (L. Wu et al., 2020). Also, in the North Sea near Denmark, Fischereit and Larsén (2020) used COAWST to assess the impacts of atmosphere-wave coupling on offshore wind resources for a full 30-years of historical climate. They found that atmosphere-wave coupling reduced the offshore wind power density on average by 1-3%, largely in agreement with L. Wu et al. (2020) at the same location. Most of the effect on wind resource reduction is due to the coupling effect at weaker-moderate wind speeds, similar to the findings of L. Wu et al. (2019) and also Varlas et al. (2018), who found an estimated 12% reduction to wind speeds when coupling.

5 Discussion

Using mesoscale coupled atmosphere-wave-ocean models in the North and Baltic Seas (Fischereit & Larsén, 2020; L. Wu et al., 2020), coupling was shown to have a small negative effect on the offshore wind energy resource at weak-to-moderate wind speeds, with little impact at higher wind speeds. Furthermore, results from Varlas et al. (2018, 2020); L. Wu et al. (2020) suggest that the feedback from the ocean and surface waves to the marine atmospheric boundary layer is less significant than the effect of air-sea interactions on the generation of surface waves.

Nevertheless, these results should be treated with caution. The coupled models that are described in this report and used to derive these results are based on a so-called sea-surface-roughness approach, which can be interpreted as a wave-informed drag model that only accounts for downward momentum transfer from the atmosphere to the ocean (Deskos et al., 2021). As mentioned in the introduction, ocean waves can impart an upward flux of momentum from the ocean to the atmosphere (Patton et al., 2019), especially under swell-dominated sea where long waves propagate in light or moderate wind conditions (Deskos et al., 2021). Notably, these are the conditions where the negative impact on offshore wind energy resources was identified in Fischereit and Larsén (2020); L. Wu et al. (2020).

Recently, Patton et al. (2019) attempted to improve the sea-surface-roughness approach under swell conditions accounting for the wave propagation angle. Here, instead of using the aerodynamic drag paradigm, they start with Andreas, Mahrt, and Vickers (2012)'s direct polynomial relationship for obtaining u_* from U_{10} (24), which was found to have better agreement across a wide range of wind speeds (better accounting for the ocean wave state) than the standard drag approach. Patton et al. (2019) then modifies this for wave-age and propagation angle in (23),

$$u_* = u_{*,A}\left[1 + \frac{\gamma C_p}{u_{*,A}}\left(1 - \cos\phi\right)\right] \tag{23}$$

$$u_{*,A} = 0.239 + 0.0433\left[(U_{10} - 8.271) + \sqrt{0.120(U_{10} - 8.721)^2 + 0.181}\right] \tag{24}$$

where ϕ is the angle between U_{10} and the propagation direction of the surface waves, and γ = 0.007 is a small dimensionless parameter. This parameterization was tested in WRF with clearly better agreement to observed wind speeds at the FINO1 North Sea tower platform, as compared to using the standard Charnock approximation. Moreover, the increased drag induced by swell propagating at directions counter to the winds was found to increase the surface drag and reduce wind speeds (Patton et al., 2019), which is in fact similar to the findings described in Sect. 4.3.

Going forward, instead of using mesoscale atmospheric models coupled with phase-averaged spectral wave models, fine-scaled large-eddy simulations (LES) of the atmosphere coupled to phase-resolved wave models (typically potential-flow solver-based) can be used to better represent the wind-wave interaction around the wind turbine (see Deskos et al. (2021) for a review). In this paradigm, the potential-flow wave model provides information regarding the free-surface vertical displacement and surface orbital velocities to the LES solver as a wavy bottom boundary condition which locally distorts the LES mesh; and the LES model passes the surface atmospheric pressure fluctuations to the potential-flow wave solver as a free surface dynamic boundary condition (Deskos et al., 2021). This two-way coupled phase-resolved framework has demonstrated improved prediction of air-sea fluxes as well as the wind input to the waves, such as the wave growth rates (Deskos et al., 2021). Still, potential-flow wave models omit viscous effects and therefore cannot simulate sea spray – which has been shown to carry a significant portion of the total vertical momentum flux at the surface as sea-spray concentrations become large (Richter & Sullivan, 2013) – or energy dissipation as a result of wave breaking (Deskos et al., 2021). To overcome this limitation,

more expensive multiphase Computational Fluid Dynamics (CFD) models which track the air-sea interface may be required (e.g., Y. Zhang & Kim, 2018).

In addition to using these fine-scaled models directly for improved analysis of offshore wind resource and turbine design, they can also be used to guide improved parameterizations for our mesoscale models. Indeed, Patton et al. (2019)'s study itself used LES simulations of the atmosphere to calibrate their parameterization shown in Eq. (23). However, their study builds the lower bottom wave boundary condition offline based on linear wave theory and an assumption of wind-wave equilibrium, and therefore the waves do not respond to local wind forcing (Patton et al., 2019). Improving bulk parameterizations with more sophisticated models that incorporate two-way interaction as outlined in Deskos et al. (2021), and using machine learning methods such as neural networks to train against observations (e.g., Gagne et al., 2020; Kosovic, McCandless, Gagne, T., & Haupt, 2020), is warranted.

References

Abdolali, A., Roland, A., van der Westhuysen, A., Meixner, J., Chawla, A., Hesser, T. J., ... Sikiric, M. D. (2020). Large-scale hurricane modeling using domain decomposition parallelization and implicit scheme implemented in WAVEWATCH III wave model. *Coastal Engineering*, *157*, 103656. Retrieved from `https://doi.org/10.1016/j.coastaleng.2020.103656` doi: 10.1016/j.coastaleng.2020.103656

Andreas, E. L., Mahrt, L., & Vickers, D. (2012). A new drag relation for aerodynamically rough flow over the ocean. *Journal of the Atmospheric Sciences*, *69*(8), 2520–2537. doi: 10.1175/JAS-D-11-0312.1

Bourdallé-Badie, R., Bell, M., Chanut, J., Clementi, E., Coward, A., Drudi, M., ... Storkey, D. (2019). *Nucleus for European Modelling of the Ocean: NEMO ocean engine* (27— ISSN ed.; Scientific Notes of Climate Modelling Center, Ed.). doi: 10.5281/zenodo.1464816

Cavaleri, L., Barbariol, F., Benetazzo, A., & Waseda, T. (2019). Ocean wave physics and modeling the message from the 2019 Wise meeting. *Bulletin of the American Meteorological Society*, *100*(12), ES297–ES300. doi: 10.1175/BAMS-D-19-0195.1

Charnock, H. (1955). Wind stress on a water surface. *Quarterly Journal of the Royal Meteorological Society*, *81*(350), 639–640. doi: 10.1002/qj.49708135026

Chen, S. S., Price, J. F., Zhao, W., Donelan, M. A., & Walsh, E. J. (2007). The CBLAST-Hurricane program and the next-generation fully coupled atmosphere-wave-ocean models for hurricane research and prediction. *Bulletin of the American Meteorological Society*, *88*(3), 311–317. doi: 10.1175/BAMS-88-3-311

Craig, A., Valcke, S., & Coquart, L. (2017). Development and performance of a new version of the OASIS coupler, OASIS3-MCT-3.0. *Geoscientific Model Development*, *10*(9), 3297–3308. doi: 10.5194/gmd-10-3297-2017

Deskos, G., Lee, J. C. Y., Draxl, C., & Sprague, M. A. (2021). Review of wind-wave coupling models for large-eddy similation of the marine atmospheric boundary layer. *Journal of the Atmospheric Sciences*, under review.

Drennan, W. M., Graber, H. C., Hauser, D., & Quentin, C. (2003). On the wave age dependence of wind stress over pure wind seas. *Journal of Geophysical Research*, *108*(C3), 8062. doi: 10.1029/2000JC000715

Fischereit, J., & Larsén, X. G. (2020). *Relevance of sea waves and farm-farm wakes for offshorewind resource assessment* (Tech. Rep.). DTU Wind Energy. Retrieved from `https://www.sintef.no/globalassets/project/eera-deepwind-2020/presentations/c2_fischereit_dtu.pdf`

Gagne, I., D. J., McCandless, T., Kosovic, B., DeCastro, A., Loft, R. D., Haupt, S. E., & Yang, B. (2020). Machine learning parameterization of the surface Layer: Integration with WRF. In *100th AGU Fall Annual Meeting.* AMS.

Haupt, S. E., Kosovic, B., Shaw, W., Berg, L. K., Churchfield, M., Cline, J., ... Sever, G. (2019). On bridging a modeling scale gap: Mesoscale to microscale coupling for wind energy. *Bulletin of the American Meteorological Society*, *100*(12), 2533–2549. doi: 10.1175/BAMS-D-18-0033.1

Jacob, R., Larson, J., & Ong, E. (2005). M × N communication and parallel interpolation in community climate system model version 3 using the model coupling toolkit. *International Journal of High Performance Computing Applications*, *19*(3), 293–307. doi: 10.1177/1094342005056116

Janssen, P. A. E. M. (1991). Quasi-linear Theory of Wind-Wave Generation Applied to Wave Forecasting. *Journal of Physical Oceanography*, *21*(11), 1631–1642. doi: 10.1175/1520-0485(1991)021⟨1631:QLTOWW⟩2.0.CO;2

Kalvig, S., Gudmestad, O. T., & Winther, N. (2014). Exploring the gap between 'best knowledge' and 'best practice' in boundary layer meteorology for offshore wind energy. *Wind Energy*, *17*, 161–171. doi: 10.1002/we.1572

Kosovic, B., McCandless, T., Gagne, I., D. J., T., B., & Haupt, S. E. (2020). Machine learning models for replacing Monin-Obukhov similarity theory based surface layer parameterization. In *100th AGU Fall Annual Meeting.* AMS.

Larson, J., Jacob, R., & Ong, E. (2005). The model coupling toolkit: A new Fortran90 toolkit for building multiphysics parallel coupled models. *International Journal of High Performance Computing Applications*, *19*(3), 277–292. doi: 10.1177/1094342005056115

Li, G., Curcic, M., Iskandarani, M., Chen, S. S., & Knio, O. M. (2019). Uncertainty propagation in coupled atmosphere-wave-ocean prediction system: A study of Hurricane Earl (2010). *Monthly Weather Review*, *147*(1), 221–245. doi: 10.1175/MWR-D-17-0371.1

Liu, B., Liu, H., Xie, L., Guan, C., & Zhao, D. (2011). A Coupled atmosphere-wave-ocean modeling system: simulation of the intensity of an idealized tropical cyclone. *Monthly Weather Review*, *139*(1), 132–152. doi: 10.1175/2010MWR3396.1

Makin, V. K. (2005). A note on the drag of the sea surface at hurricane winds. *Boundary-Layer Meteorology*, *115*(1), 169–176. doi: 10.1007/s10546-004-3647-x

Monin, A. S., & Obukhov, A. M. (1954). Basic laws of turbulent mixing in the surface layer of the atmosphere. *Contrib. Geophys. Inst. Acad. Sci. USSR*, *24*(151), 163–187.

Olabarrieta, M., Warner, J. C., Armstrong, B., Zambon, J. B., & He, R. (2012). Ocean-

atmosphere dynamics during Hurricane Ida and Nor'Ida: An application of the coupled ocean-atmosphere-wave-sediment transport (COAWST) modeling system. *Ocean Modelling*, *43-44*, 112–137. doi: 10.1016/j.ocemod.2011.12.008

Oost, W. A., Komen, G. J., Jacobs, C. M., & Van Oort, C. (2002). New evidence for a relation between wind stress and wave age from measurements during ASGAMAGE. *Boundary-Layer Meteorology*, *103*(3), 409–438. doi: 10.1023/A:1014913624535

Patton, E. G., Sullivan, P. P., Kosović, B., Dudhia, J., Mahrt, L., Žagar, M., & Marić, T. (2019). On the influence of swell propagation angle on surface drag. *Journal of Applied Meteorology and Climatology*, *58*(5), 1039–1059. doi: 10.1175/JAMC-D-18-0211.1

Powers, J. G., Klemp, J. B., Skamarock, W. C., Davis, C. A., Dudhia, J., Gill, D. O., ... Duda, M. G. (2017). The weather research and forecasting model: Overview, system efforts, and future directions. *Bulletin of the American Meteorological Society*, *98*(8), 1717–1737. doi: 10.1175/BAMS-D-15-00308.1

Richter, D. H., & Sullivan, P. P. (2013). Sea surface drag and the role of spray. *Geophysical Research Letters*, *40*, 656–660. doi: 10.1002/grl.50163

Shchepetkin, A. F., & McWilliams, J. C. (2005). The regional oceanic modeling system (ROMS): A split-explicit, free-surface, topography-following-coordinate oceanic model. *Ocean Modelling*, *9*(4), 347–404. doi: 10.1016/j.ocemod.2004.08.002

Sullivan, P. P., & McWilliams, J. C. (2010). Dynamics of Winds and Currents Coupled to Surface Waves. *Annu. Rev. Fluid Mech.*, *42*, 19–42. doi: 10.1146/annurev-fluid -121108-14554

Sutil, U. A., & Pezzi, L. P. (2020). *COAWST User's Guide* (Tech. Rep. No. 3rd Edition). San Jose do Campos: INPE. doi: 10.13140/RG.2.2.31269.12002

Taylor, P. K., & Yelland, M. J. (2001). The dependence of sea surface roughness on the height and steepness of the waves. *Journal of Physical Oceanography*, *31*(2), 572–590. doi: 10.1175/1520-0485(2001)031⟨0572:TDOSSR⟩2.0.CO;2

The SWAN team. (2020). *SWAN: Scientific and technical documentation (SWAN Cycle III version 41.31A)* (Tech. Rep.). Delft, The Netherlands: Delft University of Technology. Retrieved from `http://swanmodel.sourceforge.net/download/zip/swantech.pdf`

Varlas, G., Katsafados, P., Papadopoulos, A., & Korres, G. (2018). Implementation of a two-way coupled atmosphere-ocean wave modeling system for assessing air-sea interaction over the Mediterranean Sea. *Atmospheric Research*, *208*, 201–217. Retrieved from `https://doi.org/10.1016/j.atmosres.2017.08.019` doi: 10.1016/j.atmosres.2017.08.019

Varlas, G., Spyrou, C., Papadopoulos, A., Korres, G., & Katsafados, P. (2020). One-year assessment of the CHAOS two-way coupled atmosphere-ocean wave modelling system over the Mediterranean and Black Seas. *Mediterranean Marine Science*, *21*(2), 372–385. doi: 10.12681/mms.21344

Veers, P., Dykes, K., Lantz, E., Barth, S., Bottasso, C. L., Carlson, O., ... Wiser, R. (2019). Grand challenges in the science of wind energy. *Science*, *366*(6464). doi: 10.1126/science.aau2027

Warner, J. C., Armstrong, B., He, R., & Zambon, J. B. (2010). Development of a Coupled Ocean-Atmosphere-Wave-Sediment Transport (COAWST) Modeling System. *Ocean Modelling*, *35*(3), 230–244. doi: 10.1016/j.ocemod.2010.07.010

Wu, L., Breivik, Ø., & Rutgersson, A. (2019). Ocean-Wave-Atmosphere Interaction Processes in a Fully Coupled Modeling System. *Journal of Advances in Modeling Earth Systems*, *11*(11), 3852–3874. doi: 10.1029/2019MS001761

Wu, L., Shao, M., & Sahlée, E. (2020). Impact of air-wave-sea coupling on the simulation of offshore wind and wave energy potentials. *Atmosphere*, *11*(327). doi: 10.3390/atmos11040327

Wu, R., Zhang, H., Chen, D., Li, C., & Lin, J. (2018). Impact of Typhoon Kalmaegi (2014) on the South China Sea: simulations using a fully coupled atmosphere-ocean-wave model. *Ocean Modelling*, *131*, 132–151. Retrieved from `https://doi.org/10.1016/j.ocemod.2018.08.004` doi: 10.1016/j.ocemod.2018.08.004

WW3DG, T. W. I. D. G. (2019). *User manual and system documentation of WAVEWATCH III version 6.07* (Vol. 333; Tech. Rep.). College Park, MD, USA: NOAA/NWS/NCEP/MMAB. Retrieved from `https://www.researchgate.net/publication/336069899_User_manual_and_system_documentation_of_WAVEWATCH_III_R_version_607`

Zambon, J. B., He, R., & Warner, J. C. (2014). Investigation of hurricane Ivan using the coupled ocean–atmosphere–wave–sediment transport (COAWST) model. *Ocean Dynamics*, *64*(11), 1535–1554. doi: 10.1007/s10236-014-0777-7

Zhang, J., Huang, L., Wen, Y., & Deng, J. (2009). A distributed coupled atmosphere-wave-ocean model for typhoon wave numerical simulation. *International Journal of Computer Mathematics*, *86*(12), 2095–2103. doi: 10.1080/00207160802047632

Zhang, Y., & Kim, B. (2018). A fully coupled computational fluid dynamics method for analysis of semi-submersible floating offshorewind turbines underwind-wave excitation conditions based on OC5 data. *Applied Sciences*, *8*(11), 2314. doi: 10.3390/app8112314

Environmental Science Division
Argonne National Laboratory
9700 South Cass Avenue, Bldg. #230
Argonne, IL 60439

www.anl.gov